Probing a Chemical Compass: Novel Variants of Low-Frequency Reaction Yield Detected Magnetic Resonance.

Supporting Information

Kiminori Maeda,[a,b,‡] Jonathan G. Storey,[a,‡] Paul A. Liddell,[c] Devens Gust,[c] P. J. Hore,[d] C. J. Wedge[e,*] and Christiane R. Timmel[a,*]

[a] Department of Chemistry, University of Oxford, Centre for Advanced Electron Spin Resonance, Inorganic Chemistry Laboratory, Oxford, OX1 3QR, UK.
Email: christiane.timmel@chem.ox.ac.uk

[b] Present Address: Department of Chemistry, Graduate School of Science and Engineering, Saitama University, Shimo-okubo, Sakura-ku, Saitama 338-8570, Japan.

[c] Department of Chemistry and Biochemistry, Arizona State University, Tempe, Arizona, USA.

[d] Department of Chemistry, University of Oxford, Physical & Theoretical Chemistry Laboratory, Oxford, OX1 3QZ, UK.

[e] Department of Physics, University of Warwick, Gibbet Hill Road, Coventry, CV4 7AL, UK.
Email: c.wedge@warwick.ac.uk

[‡] These authors contributed equally to this work

Contents

1. Filtering of time-profiles

Time-profiles in RYDMR experiments contained significant RF noise due to radiation from the high power RF circuits. For sufficiently short-lived radical pairs this can be filtered from the time-profile using a boxcar algorithm with gate-width equal to the RF period of 27.8 ns. However, the transient absorption signal of the CPF triad studied here decays over a few microseconds. This means that an observation window sufficiently long to capture the entire decay necessitates a lower time-resolution which insufficiently samples the RF noise for boxcar filtering to be effective. Experimental data were manipulated using two filters: i) a second order low-pass filter with a cut-off frequency of 50 MHz (−3dB). This filter removes high-frequency noise from the spectrum. The cut-off frequency was selected as Fourier transforms of the experimental signals show only a small component above 50 MHz. ii) A 36 MHz notch filter, with $Q = 2$. This sharp filter is used to remove the RF pick-up at 36 MHz, while leaving the rest of the signal intact. Multiple comparisons between filtered and raw data confirmed that no significant distortion of the time-profiles occurred using this method.

Simulated data do not suffer from RF pickup, and so were filtered with the low-pass filter alone, to allow for an accurate comparison between the simulated and experimental data.

2. Additional experimental details

2.1. RF circuit and timing control

In order to maximize the magnitude of the oscillating field and provide an impedance match for the RF amplifier, a tuned circuit is used with parallel and series trimming capacitors adjusted to give an overall load of 50 Ω. The pulsing of the RF is controlled by a home-built synchronisation unit which gates the input from a 36 MHz frequency source (PTS-200) and the 100 W RF amplifier (Wessex RC114-100) in response to a trigger signal. The timing of this unit is controlled by two Stanford delay generators (SRS DG535). The master delay generator provides the trigger source with a 10 Hz repetition rate, which in turn triggers the laser flash lamps with a TTL pulse. The second output is delayed by 200–300 μs, providing approximately the required Q-switch delay for the laser. This pulse arms the RF gating unit which is then triggered by the next positive-going transition of the RF input, causing the RF gate to open if the computer-controlled RF flag is high. A small additional delay is then applied to allow for the rise time of the RF amplifier before a TTL pulse output triggers the laser Q-switch. The RF gate-width is sufficient to allow complete decay of the RP signal before the gate is closed. As the gating unit controls both the RF gate and the laser trigger it is possible with this setup to control the initial phase of the RF field when the RP is generated. Although the 7 ns pulse of the laser corresponds to a significant fraction of one RF period at 36 MHz, this technology allows the effect of RF phase at the moment of RP generation to be investigated at lower frequencies [J.G. Storey *et al*., manuscript in preparation]. As the phase of the RF signal is fixed relative to the laser trigger the second delay generator is used to introduce a half period (13.885 ns) delay to half of the Q-switch trigger pulses with the effect of efficiently cancelling RF interference on the signal cables.

2.2. Relative field orientation

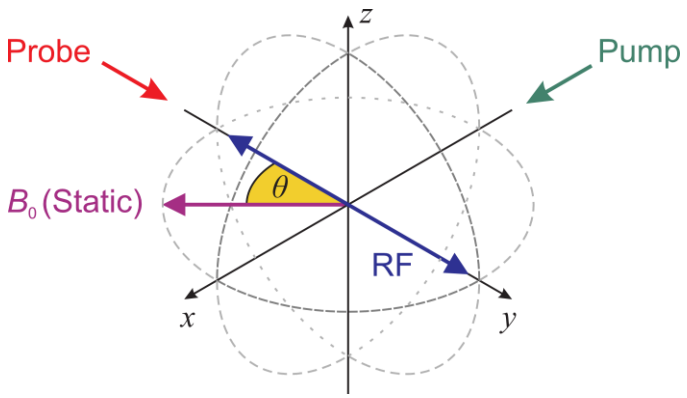

Figure S1. Relative orientations of optical excitation and magnetic fields for the RYDMR experiment, all of which lie in the horizontal plane. The pump pulse (532 nm) and probe beam (975 nm) are perpendicular, the radiofrequency oscillating field is linearly-polarised and co-linear with the probe beam. The static field direction is defined by the angle θ with respect to the RF field.

3. EPR data

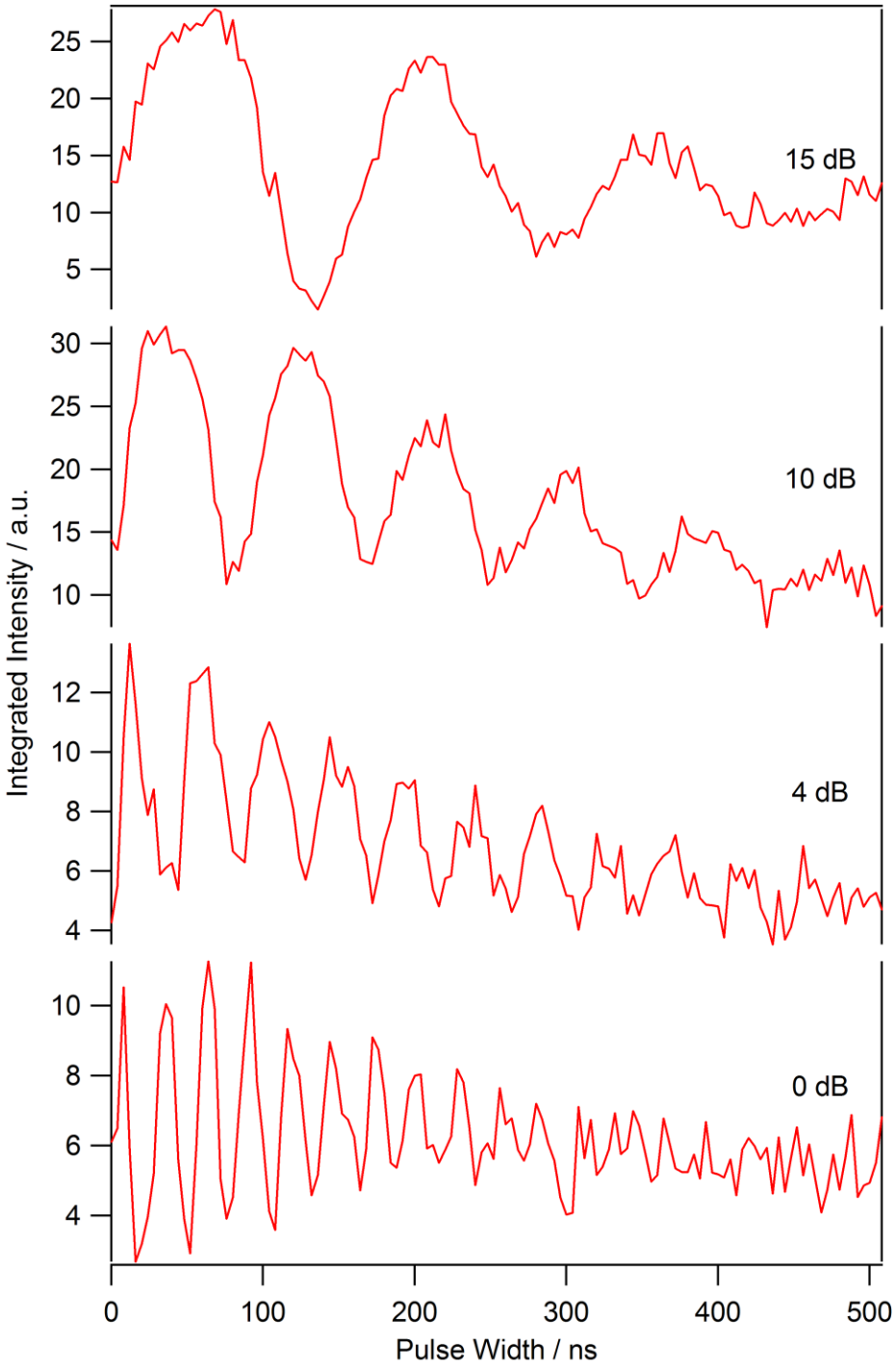

Figure S2. Transient-EPR nutation data for the CPF triad as a function of microwave attenuation. Data are presented as a function of the length of a microwave pulse applied 200 ns after the radical-generating 532 nm laser pulse. Detection is achieved by integrating the FID obtained from a π/2 pulse at a fixed time of 2 μs after the laser pulse. Experiments were performed at 110 K, B_0 = 347 mT, ν_{mw} = 9.686 GHz. Note that no double-frequency beats are observed.

4. RYDMR data

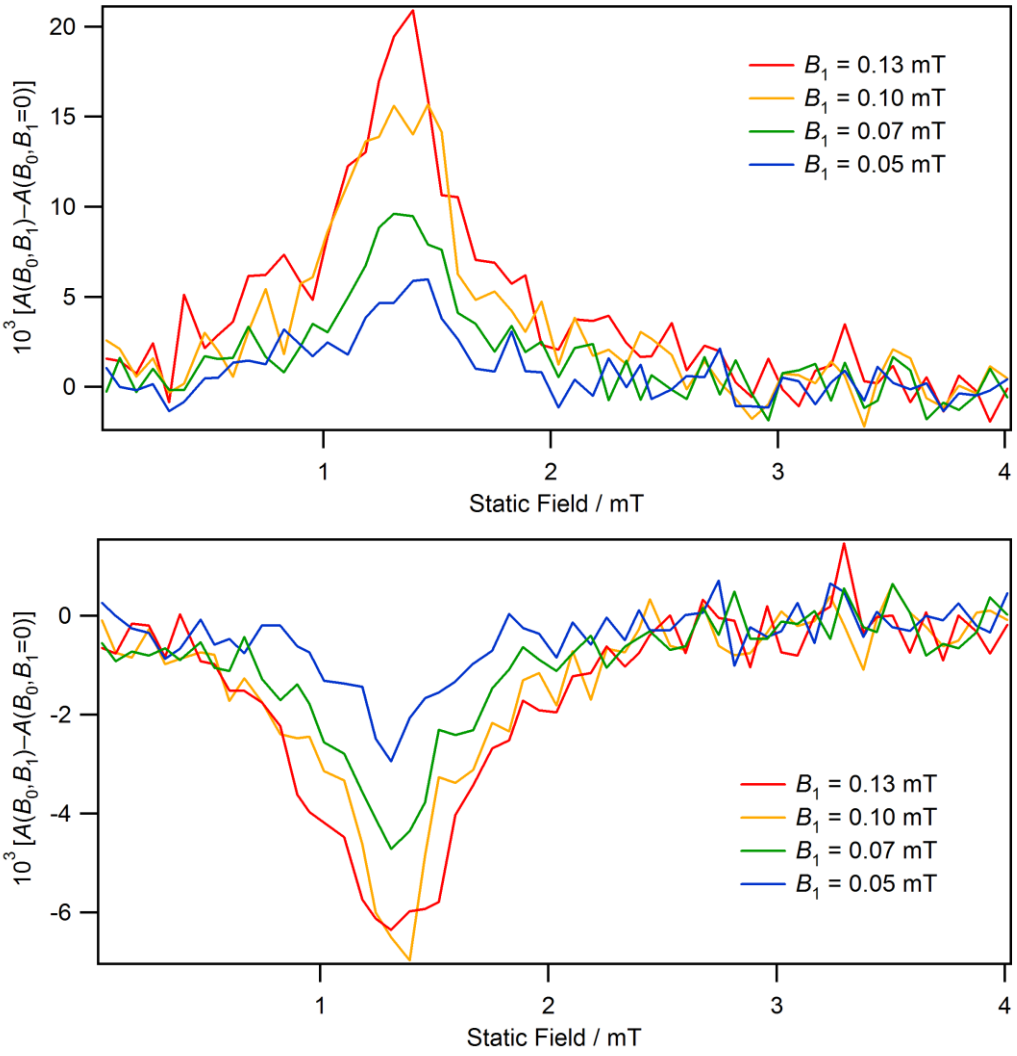

Figure S3. Time-resolved RYDMR spectra as a function of oscillating field strength as indicated. Spectra were recorded with perpendicular static and 36 MHz oscillating fields and are the result of averaging data over the range 100 to 300 ns (top) and 700 to 900 ns (bottom) after the laser flash, respectively.

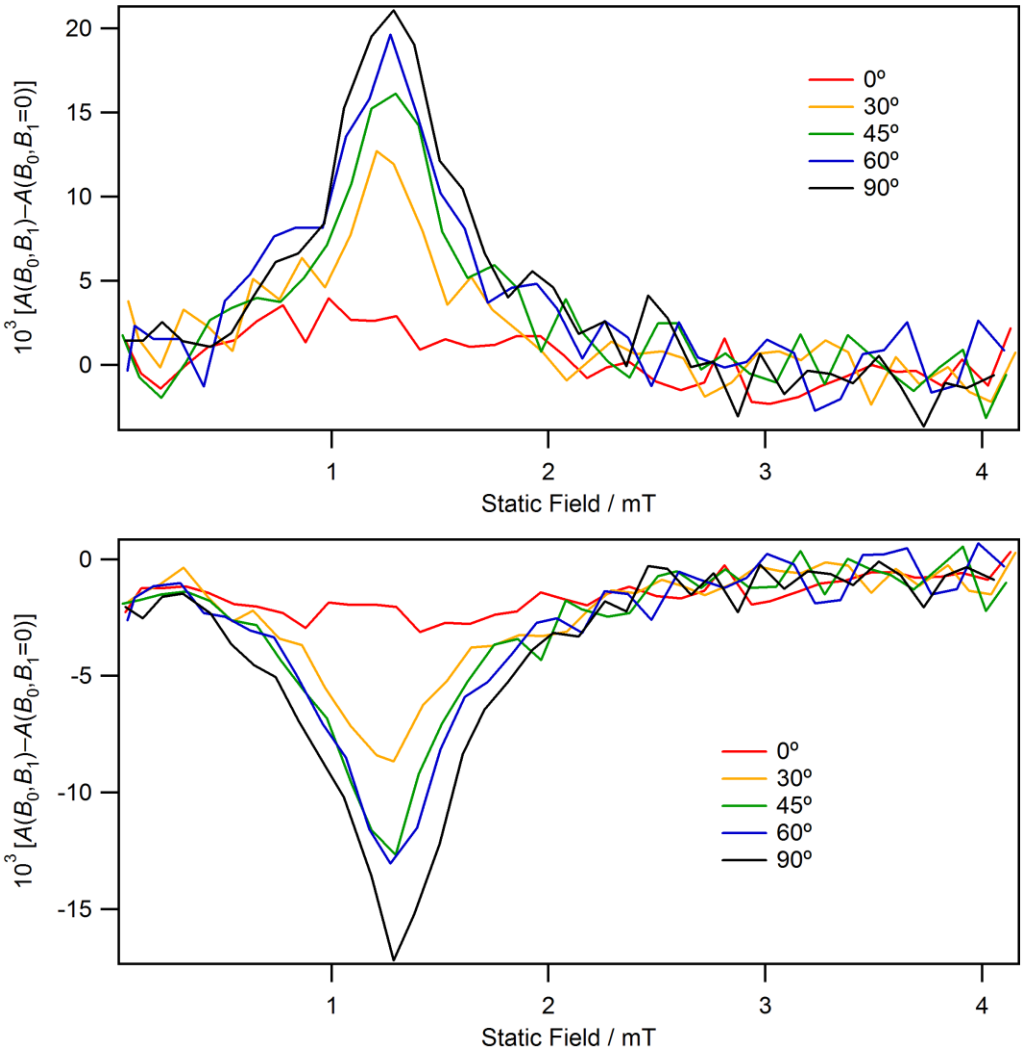

Figure S4. Time-resolved RYDMR spectra as a function of angle θ between the static and oscillating magnetic fields as indicated. Spectra are the result of averaging data over the range 100 to 300 ns (top) and 700 to 900 ns (bottom) after the laser flash, respectively. B_1 = 0.13 mT, ν_{rf} = 36 MHz.

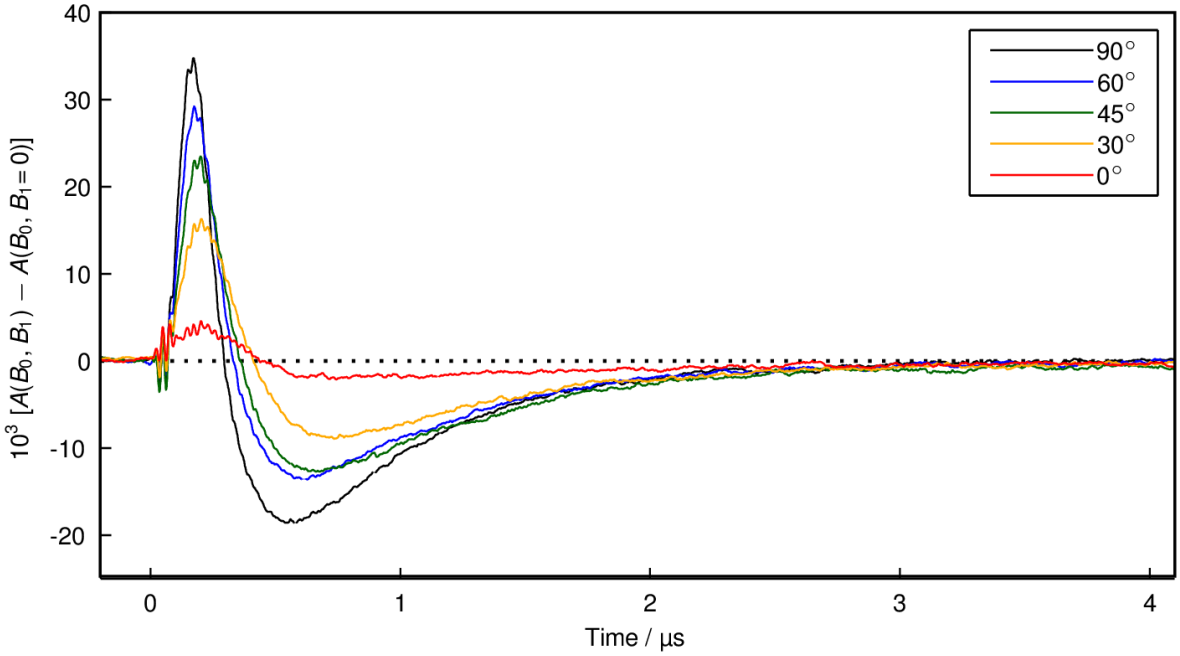

Figure S5. Transient-absorption detected RYDMR time-profiles as a function of angle θ between static and oscillating magnetic fields. In all cases a signal inversion can be observed corresponding to inversion of spin-polarization, with the time of this inversion moving to slightly later times as the fields are rotated away from perpendicular alignment which reduces the efficiency of the spin-mixing process. $B_0 = 1.28$ mT, $\nu_{rf} = 36$ MHz, $B_1 = 0.13$ mT.

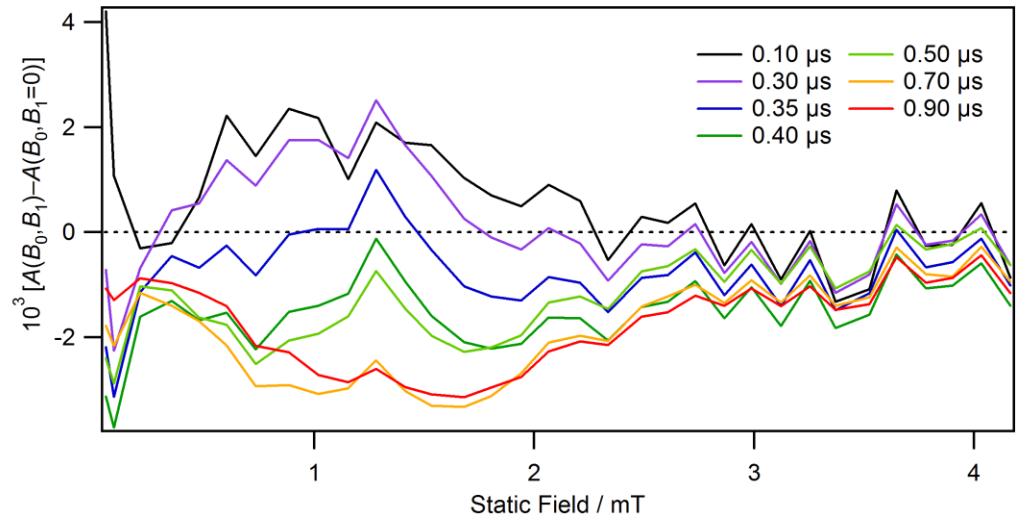

Figure S6. Time-resolved RYDMR spectra as a function of time. The centre of a 100 ns wide averaging window is as indicated. Spectra were recorded with static and 36 MHz oscillating fields parallel, $B_1 = 0.17$ mT.

5. Invariance of simulations to hyperfine couplings

Figure S7 presents simulated data for 4 different hyperfine coupling conditions. The two lines marked "Equal HFCCs" and "Unequal HFCCs" provide a check that use of identical hyperfine couplings does not produce anomalous simulation results due to degeneracy in the radical pair energy levels. "Equal HFCCs" has both hyperfine couplings set to the same value of 0.6 mT. "Unequal HFCCs" has the couplings perturbed such that the values of the couplings differ by 0.06 mT (10% of the original value), while the root-mean-square value of the hyperfine couplings remains the same. This gives HFCCs of 0.62925 mT and 0.56925 mT. These traces are virtually indistinguishable showing that, in this instance, having degenerate hyperfine couplings does not introduce anomalies.

The hyperfine couplings of the "Unequal HFCCs" case were perturbed by increasing or decreasing both values by 10%, to generate the values for the two other traces – "Larger HFCCs" and "Smaller HFCCs". In the "Larger HFCCs" case this gives hyperfine coupling constants of 0.69217 mT and 0.62617 mT, and in the "Smaller HFCCs" case the constants are 0.56632 mT and 0.51232 mT. Although these changes cause minor variations in the overall shape of the curve they verify that it is relatively insensitive to the precise hyperfine coupling constants used, and changes in the zero-crossing time of the data are significantly smaller than 10%. This insensitivity to the exact hyperfine coupling constants chosen for the simulation justifies our decision to use physically plausible values to recreate the width of the carotenoid hyperfine spectrum but not to attempt to match precisely any (or all) of the 22 significant (> 100 μT) couplings in the real radical [K. Maeda et al., *Nature*, **453**, 387–390, (2008)].

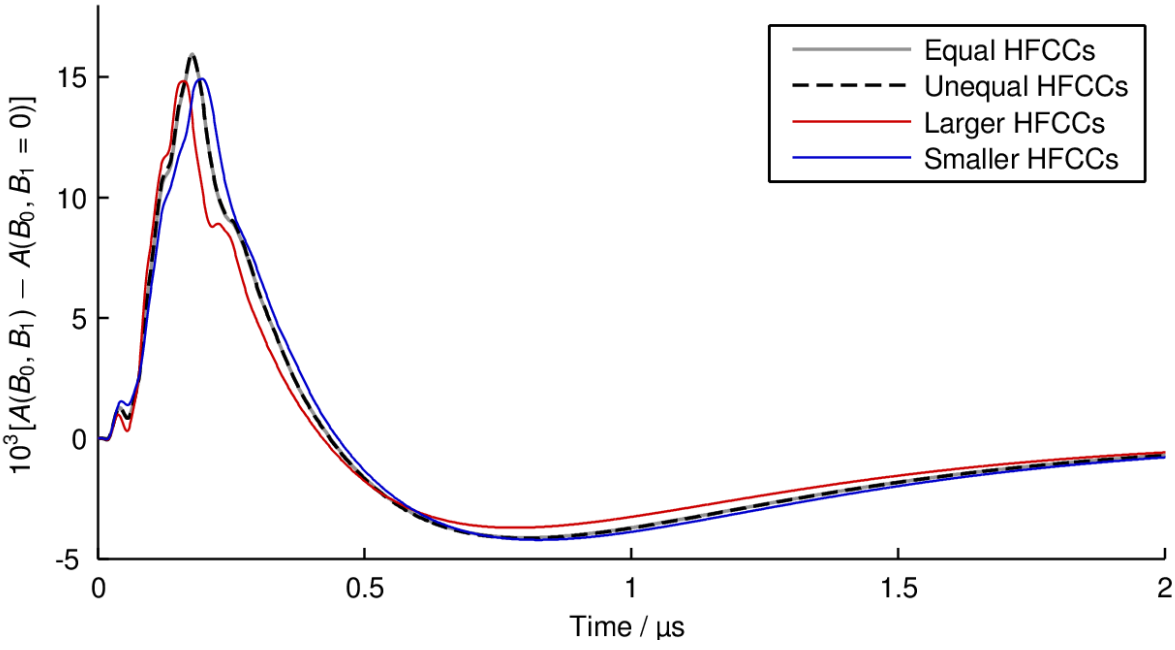

Figure S7. Simulated RYDMR time-profiles. Two hyperfine couplings are present on the same radical which are: (i) equal at 0.6 mT; (ii) unequal at 0.62925 and 0.56925 mT, which gives a 0.06mT (10%) difference in the values whilst maintaining the root-mean-square (RMS) total coupling as in (i); (iii) hyperfine couplings of 0.69217 and 0.62617mT corresponding to a 10% increase in RMS with respect to (ii), and (iv) hyperfine couplings of 0.56632 and 0.51232 mT corresponding to a 10% decrease in RMS total coupling with respect to (ii). All other parameters are as indicated in Figure 5B.